Edge turbulence imaging in the Alcator C-Mod tokamak[a)]

S. J. Zweben[b)] and D. P. Stotler
Princeton Plasma Physics Laboratory, P.O. Box 451, Princeton, New Jersey 08540

J. L. Terry, B. LaBombard, M. Greenwald, M. Muterspaugh, C. S. Pitcher, and the Alcator C-Mod Group
Massachusetts Institute of Technology, Cambridge, Massachusetts 02139

K. Hallatschek
Centre for Interdisciplinary Plasma Studies, Max-Plank-Institut für Plasmaphysik, D-85748 Garching, Germany

R. J. Maqueda
Los Alamos National Laboratory, Los Alamos, New Mexico 87545

B. Rogers
Dartmouth College, Hanover, New Hampshire 03755

J. L. Lowrance, V. J. Mastrocola, and G. F. Renda
Princeton Scientific Instruments, Monmouth Junction, New Jersey 08852

(Received 26 October 2001; accepted 28 November 2001)

The two-dimensional (2D) radial vs poloidal structure of edge turbulence in the Alcator C-Mod tokamak [I. H. Hutchinson, R. Boivin, P. T. Bonoli *et al.*, Nucl. Fusion **41**, 1391 (2001)] was measured using fast cameras and compared with three-dimensional numerical simulations of edge plasma turbulence. The main diagnostic is gas puff imaging, in which the visible D_α emission from a localized D_2 gas puff is viewed along a local magnetic field line. The observed D_α fluctuations have a typical radial and poloidal scale of $\approx$1 cm, and often have strong local maxima (''blobs'') in the scrape-off layer. The motion of this 2D structure motion has also been measured using an ultrafast framing camera with 12 frames taken at 250 000 frames/s. Numerical simulations produce turbulent structures with roughly similar spatial and temporal scales and transport levels as that observed in the experiment; however, some differences are also noted, perhaps requiring diagnostic improvement and/or additional physics in the numerical model. © *2002 American Institute of Physics.* [DOI: 10.1063/1.1445179]

I. INTRODUCTION

Turbulent plasma fluctuations have been observed at the edge of tokamaks for many years, both inside and outside the last closed magnetic flux surface, as described in the reviews of Refs. 1–3. However, despite a wealth of experimental data there is little direct quantitative or even qualitative understanding of these measurements in terms of the basic theory of edge plasma turbulence, which has advanced rapidly in the past few years.[4–7]

The present experiment was motivated by recent advances in the theoretical modeling of edge turbulence; in particular, by the two-dimensional (2D) turbulence structure calculated from three-dimensional (3D) nonlinear simulation codes.[4,5] These computations now look so ''realistic'' that it seems worthwhile to directly compare their results with measurements. Since the turbulence correlation length along the magnetic field is comparable to the circumference of the tokamak ($L_\parallel \approx qR$), the most interesting turbulent structure is in the radial vs poloidal plane, i.e., perpendicular to the total magnetic field. Such a comparison of experiment and theory should provide confirmation of the physical mechanisms which govern the growth, saturation, and transport effects of edge turbulence in tokamaks.

Information about the 2D structure of plasma edge turbulence in tokamaks and stellarators has been obtained for many years using statistical two-point correlation techniques, from which it has been determined that the turbulence structure is approximately isotropic in the radial vs poloidal plane with a size typically $k_\perp \rho_s \approx 0.1$, i.e., somewhat longer than the typical drift wave scale length.[1–3] The relative fluctuation level in the edge plasma is generally large ($\tilde{n}/n \geqslant 10\%$) compared to relatively small turbulence levels near the core ($\tilde{n}/n \approx 0.1\text{–}1\ \%$).[3]

The present paper describes 2D imaging of edge turbulence in which both the radial and poloidal structure is measured at one instant of time rather than inferred from statistical correlations. Such imaging techniques are often used in fluid turbulence experiments, e.g., to detect large scale ''coherent structures'' in turbulent flows.[8] Previous 2D images of edge turbulence were made using a 64-point Langmuir probe array[9] and a 32-point 2D array of beam emission spectroscopy (BES).[10] The present gas puff imaging (GPI) diagnostic has over 1000 active pixels and an optical resolution of

[a)]Paper UI1 4, Bull. Am. Phys. Soc. **46**, 322 (2001).
[b)]Invited speaker.

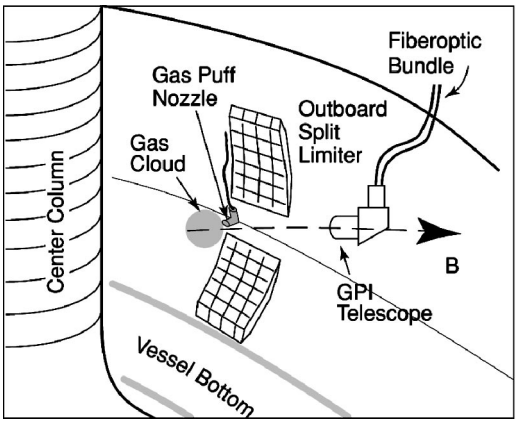

FIG. 1. Schematic view of gas puff imaging (GPI) diagnostic on Alcator C-Mod. The neutral deuterium gas enters the chamber radially through a gas puff nozzle and its D_α emission is viewed along a magnetic field line by the GPI telescope on the outer wall about 50 cm away. The 2D images of light emission from the gas puff are transferred through a coherent fiber optic bundle and D_α line filter to cameras located at the top of the machine.

≈2–3 mm, so in principle can provide the best imaging of tokamak turbulence to date.

II. GAS PUFF IMAGING DIAGNOSTIC

The general diagnostic setup and initial results for gas puff imaging of edge turbulence have already been described in papers from the National Spherical Torus Experiment (NSTX)[11] and Alcator C-Mod.[12] In this section we briefly describe the imaging system, the interpretation of these images, and other possible diagnostic issues. Although both D_2 and He gas puffs have been used on C-Mod with qualitatively similar results, for simplicity only the D_2 results will be presented in this paper.

A. Imaging system

A schematic view of the GPI diagnostic in Alcator C-Mod is shown in Fig. 1. Neutral deuterium gas is puffed radially into the edge plasma through a 3 mm diameter nozzle located ≈3 cm outside the last closed flux surface and 2.5 cm below the outer midplane. The gas is typically puffed steadily during ≈0.5–1.0 s after breakdown with a flow rate $\approx 10^{19}$–10^{20} atoms/s, which is <1% of the total ionization rate[13] and thus does not perturb the discharge as a whole.

As shown in Fig. 1, this gas puff is viewed by an imaging telescope aimed at the puff from a direction along the local magnetic field line (11° from toroidal). This provides a viewing area of ≈6 cm×6 cm in the radial vs poloidal plane centered near the magnetic separatrix ≈2.5 cm below the outer midplane. These images are transferred by a 400 ×400 coherent fiber optic bundle through a D_α (656 nm) line filter and recorded by a fast-gated intensified camera at 60 frames/s. The spatial resolution of this whole system is typically ≈2–3 mm at the gas puff plane. The D_α light emission from this puff was also recorded by three fast photodiodes viewing the same puff from the toroidal direction,[12] and sometimes by an ultrafast framing camera (see Sec. III D).

Typical images from this diagnostic are shown in Fig. 2.

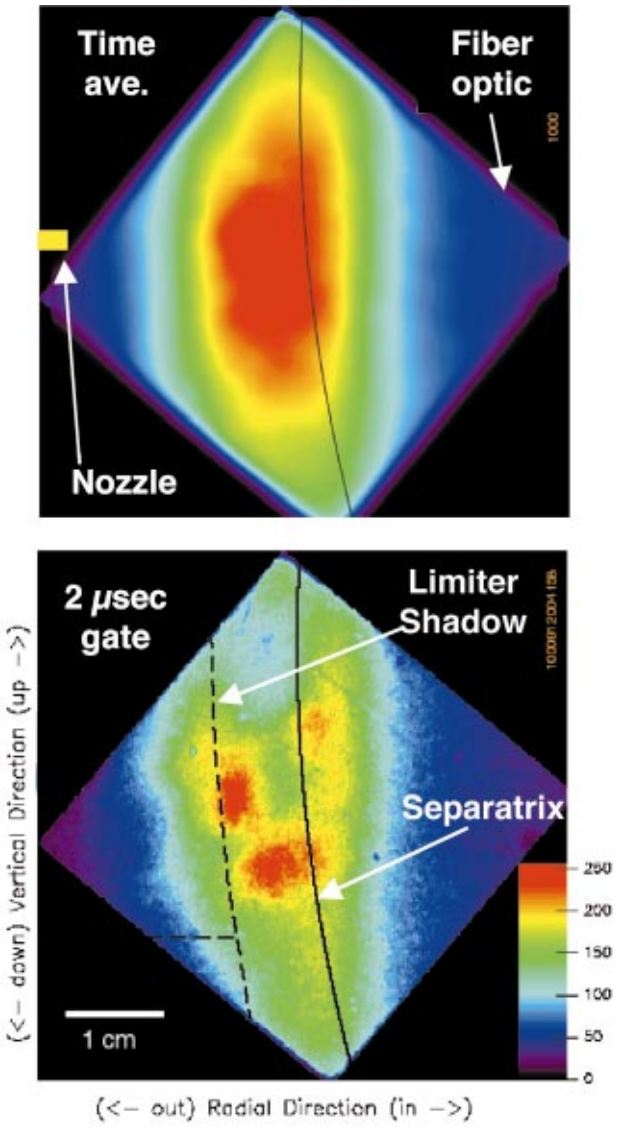

FIG. 2. (Color) Typical 2D GPI images showing the D_α light emission from the gas puff nozzle (left) as viewed through the optical fiber bundle. At the top is the time-averaged envelope of the D_α light emission summed over many frames during a typical C-Mod discharge ($B=5.3$ T, $I=0.7$ MA, #1000912004). At the bottom is a single frame from that same shot taken at an exposure time of 2 μs showing the instantaneous 2D structure of the D_α light emission, along with the locations of the magnetic separatrix and the limiter shadow in this region (dashed line). The poloidal direction is vertical and the plasma center is toward the right. The limiter is 1 m along the *B*-field line from the GPI cloud in one direction and 2 m away in the other direction.

For reference, at the top is the time average of the D_α emission, along with the location of the nozzle, and at the bottom is a single frame exposed for 2 μs, along with the location of the magnetic separatrix and limiter shadow. The irregular cm-scale structures within this 2 μs image represent the edge turbulence as viewed by GPI. This small-scale turbulence can be seen within the area of the time-averaged D_α emission ''cloud'' which extends ≈6 cm poloidally and 3 cm radially (from $\rho \approx 2$ to -1 cm, where ρ is the distance outside the separatrix). In the region outside the separatrix but inside the limiter shadow, the parallel connection length to the wall is $L_\parallel \geqslant 10$ m, while outside the limiter shadow the nearest lim-

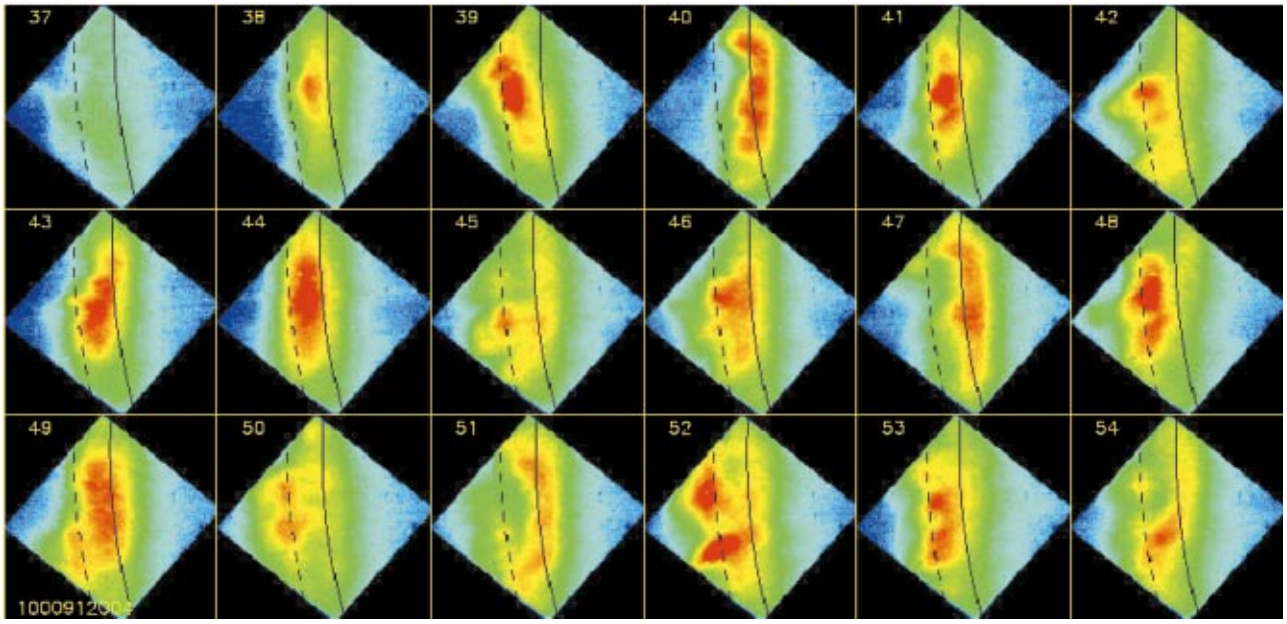

FIG. 3. (Color) Example of a sequence of GPI images in D_α light emission taken with a 2 μs exposure in standard C-Mod ohmic discharge with $B=5.3$ T and $I=0.7$ MA (#1000912004). The first frame at the upper left (#37) was taken at 0.42 s and the framing rate was 60 frames/s. The first frame shows the D_α background level just before the start of the D_2 gas puff. The color scale is the same as for Fig. 2.

iter is ≈2 m away along the *B*-field line on one side and ≈1 m away on the other side.

Figure 3 shows a set of 18 consecutive images from the same shot, each with an exposure time of 2 μs. The details of the small-scale structure of the light emission vary from frame-to-frame (at 60 frames/s), as expected for this edge turbulence with an autocorrelation time of ≈10–20 μs. The background D_α recycling light, as seen in the first frame, has a radial location similar to that of the GPI emission,[13] but a brightness level which is ≈5–10 lower than that during the D_2 GPI puff.

B. Interpretation of images

The identification of D_α light fluctuations with edge density fluctuations is motivated by several previous measurements. For example, a locally high coherence was observed between the light fluctuations and ion saturation current fluctuations in a nearly Langmuir probe,[14] and the spatial structure and frequency spectrum of D_α fluctuations from a gas D_2 puff were similar to Langmuir probe ion saturation current fluctuations.[15] Short exposure time video images of recycling light and gas puff clouds in the Tokamak Fusion Test Rector (TFTR),[16] NSTX,[11] and other devices have shown turbulent ''filaments'' of light emission which are highly elongated along the magnetic field line, as expected for structure of edge density turbulence. Previous measurements in Alcator C-Mod showed that D_α light fluctuations in this gas puff had a frequency spectrum similar to a Langmuir probe, and fast 2D toroidal vs poloidal images of the recycling light had a filament structure approximately aligned along the *B* field.[12,17]

For a quantitative interpretation of GPI light fluctuations, the local D_α emissivity needs to be evaluated from the atomic physics of deuterium atoms. In the collisional radiative approximation, ignoring recombination,

$$S_{D_\alpha}(\text{photons/cm}^3) = n_0 f(n_e, T_e) A_{3\to 2}, \tag{1}$$

where n_0 is the local deuterium atom density, and $A_{3\to 2}=4.41\times 10^7\ \text{s}^{-1}$ is the radiative decay rate from the $n=3$ to $n=2$ excited electron state. The function $f(n_e, T_e)$ gives the ratio of the density of the $n=3$ state to the ground state and is obtained from the solution of model equations balancing collisional and radiative processes affecting individual excited states. The time scale for emission of this spectral line once the atom has been excited is $1/A_{3\to 2}=0.02$ μs, i.e., much shorter than typical turbulence time scales in this experiment. This interpretation of D_α fluctuations is similar to BES,[10] except in BES the neutrals come from a neutral beam and the excitation of D_α comes from ions instead of electrons.

The DEGAS 2 code[18] has been run to determine the relationship of the D_α emission to assumed variations in the edge n_e and T_e. The transport of the puffed gas and the neutral atomic physics have been simulated in a 2D model using plasma profiles mapped onto magnetic flux surfaces for a typical shot ($B=5.4$ T, $I=1.0$ MA #1010622006). The average electron temperature and density profiles are obtained from the near-midplane reciprocating probe data; plasma parameters are taken to be constant on a flux surface. The atomic physics is the same as in Ref. 18 except that neutral–neutral collisions can be ignored here. The relevant hardware components in the simulation are the gas puff nozzle, which is a tube of 0.3 cm diameter located ≈3 cm outside the separatrix at $z=-2.5$ cm, and the outer limiter locations illustrated in Fig. 1. The calculated D_2 molecule density falls off by a factor of 10 within 1.5 cm of the nozzle tip as the molecules are dissociated into atoms (note that the

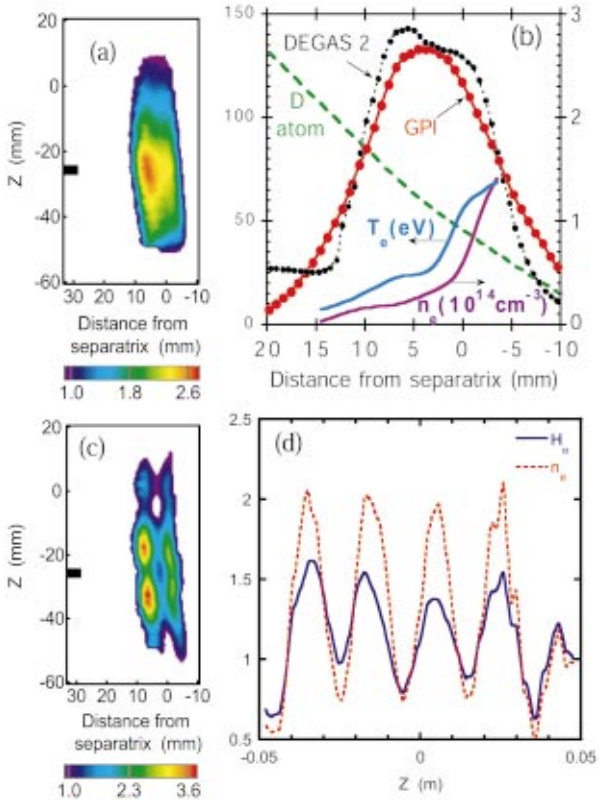

FIG. 4. (Color) DEGAS 2 simulations of the D_α light emission from the GPI gas puff nozzle. In part (a) is the 2D pattern of the time-averaged D_α emission as calculated for the measured density and temperature profiles shown in part (b), where the location of the gas puff nozzle is shown by the small rectangle at $z=-2.5$ cm in (a). Part (b) also shows a comparison of the measured (red) and calculated (black) radial profiles of D_α emission, and the calculated neutral D atom density profile (green), all at $z=-3.5$ cm. Part (c) shows the calculated D_α emission pattern with an assumed 2D perturbation in the electron density, and part (d) is a vertical slice through the perturbed GPI cloud of part (c) at 0.7 cm outside the separatrix, showing how the calculated D_α emission follows the perturbed n_e (both normalized to their unperturbed values).

D_α photons from the decay of excited atoms created during dissociation have not yet been included in these simulations).

Typical results from DEGAS 2 are illustrated in Fig. 4. In Fig. 4(a) is the time-averaged 2D emission pattern of the D_α light from the D_2 gas puff emitted by the nozzle (small black rectangle at the left), as calculated for the measured density and temperature profiles shown in Fig. 4(b). Figure 4(b) also shows a comparison of the calculated and GPI-measured radial profiles of D_α at $z=-3.5$ cm, which agree well with each other. Also shown in Fig. 4(b) is the neutral D atom radial profile at $z=-3.5$ cm, the poloidal extent of which is $\approx$4.7 cm FWHM (full-width-half-maximum) near the D_α peak at $\rho\approx 0.5$ cm outside the separatrix, where the calculated density is $\approx 2\times 10^{11}$ atoms/cm^3 for an assumed D atom influx rate of 10^{19} atoms/s. Figure 4(c) shows the calculated D_α emission cloud with an assumed 2D perturbation of 50% in the electron density, and Fig. 4(d) compares the n_e and D_α profiles in a vertical slice through Fig. 4(c) near the center of the GPI cloud, showing that the normalized fluctuations in D_α are about half the size of the amplitude of those in n_e.

The sensitivity of the D_α light emission to variations in the assumed electron density and temperature was evaluated using the collisional radiative model for atomic deuterium in DEGAS 2. The edge plasmas in Alcator C-Mod typically have 10^{13} cm$^{-3}<n_e<10^{14}$ cm^{-3} and 10 eV$<T_e<$50 eV.[17] Under these conditions, DEGAS 2 modeling shows that $S_{D_\alpha}\propto n_e^{0.5}T_e^{0.5}\propto p_e^{0.5}$ near the center of the GPI emission cloud at $\rho=0.5$ cm where $T_e\approx 25$ eV and $n_e\approx 3\times 10^{13}$ cm^{-3}. Therefore, in this case, the relative fluctuation level in S_{D_α} should be $\approx$0.5 times the relative density fluctuation level at that location, at least for small fluctuations. At the innermost point of the GPI cloud at $\rho=-0.35$ cm this sensitivity is $S_{D_\alpha}\propto n_e^{0.5}T_e^{0.3}$, while at the outermost point at $\rho=1.4$ cm the sensitivity is roughly $S_{D_\alpha}\propto n_e^{0.8}T_e^{1.4}$. A quantitative interpretation of the GPI fluctuations of S_{D_α} should therefore take into account the local density and temperature, the ratio of the local density fluctuations to the local electron temperature fluctuations, and the nonlinear effects due to large fluctuations.

For simplicity, the GPI images described in this paper will be analyzed without attempting to convert the D_α fluctuations into local electron density or temperature fluctuations, since the ratio and phase of these two fluctuating quantities is not yet measured in C-Mod. There is recent evidence from Langmuir probe measurements in TEXT that edge density temperature fluctuations are in phase and of similar relative magnitudes and spectrum,[19] in which case the interpretation would be relatively straightforward. Further development of the DEGAS 2 modeling and analysis of GPI fluctuations will be described in a future publication.

C. Other diagnostic issues

In the interpretation above it is assumed that the neutral density n_0 does not itself have significant fluctuations within the GPI emission region, e.g., due to some nonuniformity in the flow from the nozzle. This is justified since the neutral hydrogen atom density comes from the dissociation of D_2 molecules within $\approx$1 cm of the tip of the nozzle (Sec. II B), after which the D atoms travel without self-collisions into the plasma, thus forming a spatially uniform distribution in the region of D_α emission. Even without such dissociation (e.g., for He puffs), experiments on gas flow through nozzles into vacuum have shown a very smooth spatial distribution,[20] most likely due to the collisionless flow just past the nozzle. There is, however, a possible radial ''shadowing'' effect by which fluctuation-induced ionization of incoming neutrals can transiently reduce the neutral density farther toward the plasma center, similar to the edge effect in BES.[10] Although this effect is not noticeable in the GPI images (perhaps due to charge exchange), it needs to be investigated further using DEGAS 2 simulations.

Another assumption is that the GPI gas puff does not perturb the local edge turbulence being imaged. This was verified empirically in three ways: first, by observing that the frequency spectrum of the GPI D_α fluctuations as measured by the fast diodes is very similar to spectrum of ion saturation current fluctuations in a Langmuir probe at the same radius, as shown in Fig. 5; second, by observing that the

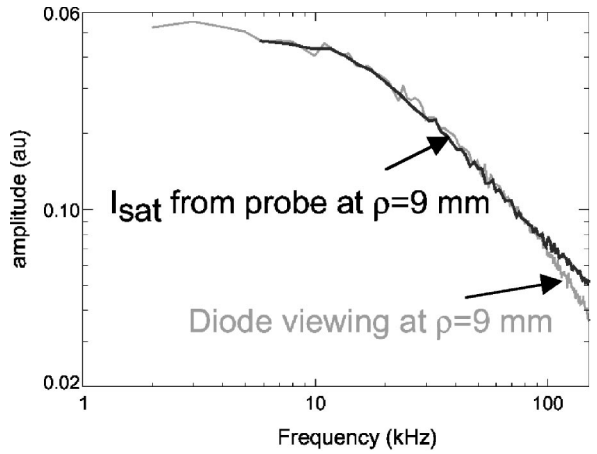

FIG. 5. Frequency spectra of D_α light fluctuations as measured by a fast diode compared with the spectrum of ion saturation current fluctuations in a Langmuir probe at the same radius ($\rho = 0.9$ cm). The diode viewed the GPI gas cloud toroidally using optics located just below the GPI telescope which had $a \approx 3$ mm viewing diameter at the gas cloud. The vertical axis is the amplitude of the fluctuations (i.e., square root of the autopower spectrum), and the two traces are normalized vertically to each other. Typical fluctuation autocorrelation times are $\tau_{\text{auto}} \approx 10-20$ μs FWHM.

spatial structure, frequency spectrum, and relative fluctuation levels of the GPI light emission did not vary significantly when the gas flow rate varied from $\approx 10^{19}$ atoms/s to $\geqslant 10^{20}$ atoms/s; and third, by observing that there was no significant change in the fluctuations seen by the Langmuir probe at the same minor radius as the GPI cloud with and without the gas puff present. This absence of a local perturbation is plausible since the radiated power from this gas puff is $\leqslant 1$ kW, and, although the local ionization rate within the GPI gas puff is up to ≈ 10 times the local recycling ionization rate, the puff contributes $<10\%$ to the total particle source averaged over a typical ≈ 10 m long connection length just outside the separatrix. Also, no effect of strong H_2 or He gas puffing on the local edge turbulence was observed in experiments in Princeton Beta Experiment Modification (PBX-M).[21]

Although the spatial resolution of the optical system is $\approx 2-3$ mm for a test pattern located at the gas puff, there can be a loss of resolution if the optical sight line is not along the parallel direction of the turbulence. If the parallel wavelength of the turbulence along the magnetic field is $\approx qR$, then this blurring should be <1 mm when viewing along a field line. If the view is slightly misaligned with the field line there will be an additional ≈ 1 mm blurring for every degree of misalignment, since the length of the GPI neutral gas cloud along the sightline is ≈ 6 cm FWHM. Thus typical variations in the local field line of up to $\approx 2°$ will cause the spatial resolution to be up to $\approx 3-4$ mm in the poloidal direction, but this resolution is still small compared to the mean correlation length of the turbulence.

III. EXPERIMENTAL RESULTS

In this section we analyze the structure of the edge turbulence as observed in the D_α light emission measured by the GPI diagnostic described in Sec. II. All the data in this paper were taken using deuterium gas puffing into deuterium-fueled C-Mod discharges without ion cyclotron resonsance heating (ICRH) heating. Typical parameters of C-Mod and its edge plasma are in Table I.

TABLE I. C-Mod parameters (# 1010622006).

Global/Core	Plasma edge[a]
$B = 5.4$ T	$n = 2.5\times10^{13}$ cm^{-3}
$I = 1.0$ MA	$T_e = 24$ eV
$R = 67$ cm	$\rho_s \approx 2.6\times10^{-2}$ cm
$a = 22$ cm	$\alpha_d \approx 0.35$
$n(0) = 1\times10^{14}$ cm^{-3}	$\alpha_{\text{mhd}} \approx 0.03$
Te(0) = 1.5 KeV	$\beta_e \approx 3\times10^{-5}$
$q_{95} \approx 3.8$	$L_{ei}/L_\parallel \approx 0.1$

[a]0.5 cm outside separatrix near outer midplane.

A. Overview

Typical GPI images of edge turbulence of C-Mod discharges were shown in Figs. 2 and 3. These images were taken with a gating time of 2 μs/frame at 60 frames/s during the steady-state part of the discharge from $\approx 0.5-1$ s after breakdown. The exposure time of 2 μs/frame was chosen to capture most of the measured frequency spectrum which, as shown in Fig. 5, was mainly below $f = 150$ kHz. Images taken at a gating time of 0.5 μs looked similar, as expected.

As viewed by eye, images such as those in Fig. 3 show random-looking spatial patterns over the ≈ 6 cm poloidal by ≈ 3 cm radial size of the GPI light emission cloud. On average, the small-scale structure within this cloud looks approximately isotropic in the poloidal vs radial plane (see Sec. III C). There is almost never any periodic structure, but there are often isolated ''blobs'' of bright emission of size ≈ 1 cm (see Sec. III D). These trends are consistent with the edge turbulence seen in previous experiments; for example, the intermittent ''blobs'' have been identified in Langmuir probe data[9,12,17] and are very also likely the ''filaments'' seen in high speed imaging of D_α.[11,16]

B. Radial profiles for a typical case

The top part of Fig. 6 shows the radial profile of the mean poloidal correlation length L_{pol} for the D_α fluctuations for the discharge of Fig. 4(b). These L_{pol} are calculated as the time average over 21 frames (0.6–0.93 s) of the FWHM of the radially resolved poloidal autocorrelation functions for each frame. Before performing the autocorrelation functions, each frame is first normalized by the time-averaged GPI image to remove the artificial variations due to the finite vertical and horizontal extent of the cloud (a 2-D spatial averaging over ≈ 1 mm is also applied to the time-averaged image). Poloidal autocorrelation functions are then computed from contiguous vertical columns in each frame, where each column is ≈ 1 mm wide (radially) and ≈ 5 cm high (poloidally). Note that the separatrix was stationary to within ≈ 2 mm during this time period, and corrections due to the ± 1 mm curvature of the separatrix were neglected in this analysis. The error bars in Fig. 6 represent typical rms deviations from these mean correlation lengths over the frames in this shot.

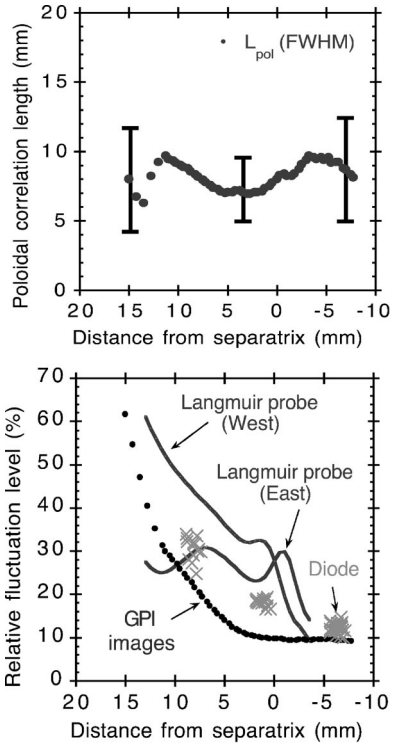

FIG. 6. Analysis of the GPI images for a typical C-Mod shot with $B=5.4$ T and $I=1.0$ MA (#1010622006). At the top is the poloidal correlation length $L_{\rm pol}$ as a function of radius averaged over 21 frames in this shot. At the bottom are the rms/mean fluctuation levels from the ion saturation currents of two electrodes on a scanning Langmuir probe, from the three discrete chords of D_α light emission measured by the fast diodes, and from the spatial deviations from the mean in the vertical slices of the normalized GPI image data used to calculate the poloidal correlation lengths.

The bottom part of Fig. 6 shows the profiles of the rms fluctuation levels (normalized to their mean) for the ion saturation currents vs time of two electrodes on a scanning Langmuir probe, from the three discrete chords of the GPI D_α light emission measured vs time by the fast diodes, and from the vertical slices of the normalized GPI image data used to calculate the poloidal correlation lengths. The Langmuir probe data agree fairly well with the fast diode data, especially considering that the relative D_α light fluctuations are not expected to have the same amplitude as the local density fluctuations (see Sec. II B). The fluctuation profile of the GPI image data is similar to the other methods even though it was based on a limited set of spatial averages and not time series.

The result of this analysis is that the mean poloidal correlation length is approximately $L_{\rm pol}\approx 0.85\pm 0.2$ cm within the range of the GPI diagnostic from $\rho=1.5$ cm outside to $\rho\approx -0.5$ cm inside the separatrix, where the density fluctuation level is roughly $\tilde{n}/n\approx 10-50\%$. This average size scale corresponds to a half-width–half-maximum (HWHM) for the k-spectral amplitude of $k_{\rm pol}\approx 3.9/L_{\rm pol}\approx 5\ {\rm cm}^{-1}$ (assuming a Gaussian correlation function), or roughly $k_{\rm pol}\rho_s\approx 0.1$, which is similar to other measurements of edge turbulence.[1,2] The $k_{\rm pol}$ spectrum is discussed in Sec. IV in connection with the theoretical simulations.

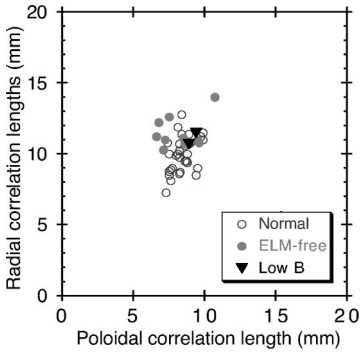

FIG. 7. Estimates of the average poloidal and radial correlation lengths $L_{\rm pol}$ and $L_{\rm rad}$ in the edge region from GPI for a variety of discharge conditions in C-Mod. The open circles are for normal operating conditions of $B\approx 5$ T, $I\approx 0.7-1.0$ MA. The closed circles are during an ELM-free H-mode discharge with $B\approx 4$ T, $I=0.8$ MA, and the triangles are for a low $B=2.8$ T, $I=0.4$ MA. In all cases the correlation lengths are $L_{\rm pol}\approx 0.85\pm 0.2$ cm and $L_{\rm rad}\approx 1.0$ cm (both FWHM), with no significant variation among discharge types.

C. Variation of correlation lengths with plasma conditions

Figure 7 shows the variation of the mean poloidal and radial correlation lengths $L_{\rm pol}$ and $L_{\rm rad}$ for a variety of discharges in Alcator C-Mod. In all cases the poloidal correlation lengths were averaged over a fixed range of radii $R=87.6-90.6$ cm near the outer separatrix (i.e., the same range as in Fig. 6), using only regions where the GPI light level was well above the background level. Note that these estimates of $L_{\rm rad}$ (as calculated in the same way as $L_{\rm pol}$ but for horizontal slices) are more uncertain than those for $L_{\rm pol}$ since the radial width of the D_α emission region is only $\approx 2-3$ times larger than $L_{\rm rad}$ (compared to ≈ 6 times larger for $L_{\rm pol}$).

Most of the points shown in Fig. 7 were for ohmic plasmas with $B=5.4$ T, $I=1$ MA or $B=5.3$ T, $I=0.7$ MA, where the mean poloidal correlation lengths were $L_{\rm pol}\approx 0.85\pm 0.2$ cm and $L_{\rm rad}\approx 1$ cm. Other types of ohmic plasma had a similar $L_{\rm pol}$, as shown for the low B cases with $B=2.8$ T, $I=0.42$ MA (at a similar edge q). No significant change was seen either with varying plasma density or with ICRH heating (not shown). Figure 7 also shows no significant change for ELM-free H-mode discharges; however, these measurements were made well outside the transport barrier, which in C-Mod is typically at $T_e\approx 200$ eV. In contrast, a clear narrowing of the radial width of the GPI (HeI) light emission in H-mode was recently seen NSTX[23] where the neutrals penetrated into the transport barrier region. On the other hand, reflectometry measurements in ASDEX-Upgrade showed no significant difference in the radial correlation length between L and H modes even within the transport barrier region.[22]

D. 2D motion of edge turbulence structure

Using the same GPI optical system as described in Sec. II, a Princeton Scientific Instruments Model PSI-3 Ultra-fast Framing Camera[24] was used to image the motion of the C-Mod edge turbulence at 250 000 frames/s. This camera

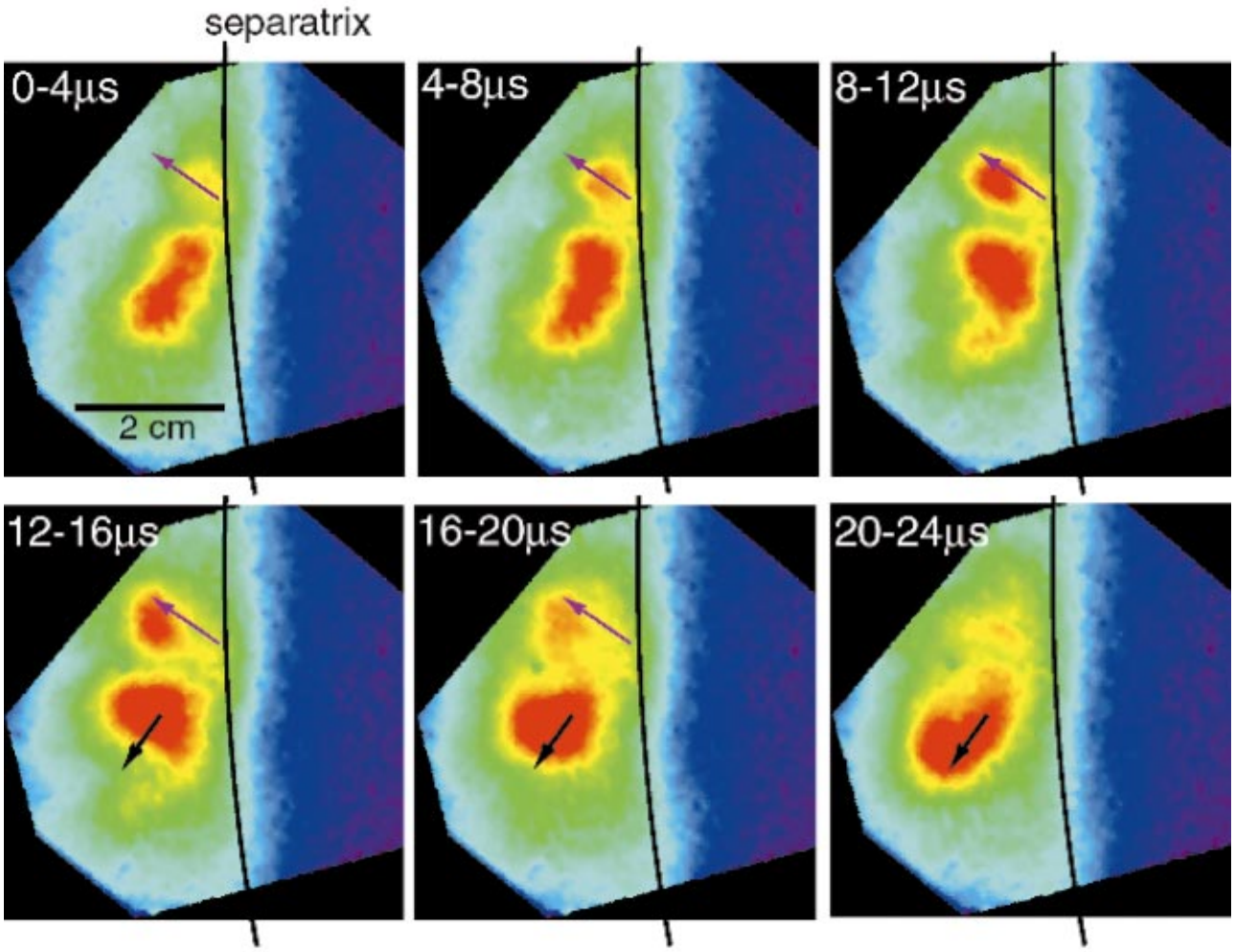

FIG. 8. (Color) Images of edge turbulence taken with the PSI camera at 4 μs/frame and 250 000 frames/s using the same view as in Fig. 2. The movement of two locally bright ''blobs'' is tracked over several frames showing their velocity of up to $\approx$1 cm/20 μs. The radially outward direction is to the left and the ion grad-B and ion diamagnetic direction is downward in these images. The arrows are shown at fixed positions for reference.

accumulates charge in each of its 64×64 pixels and stores this charge in a set of 12 sites adjacent to each pixel. Thus 12 frames can be captured during a shot and read out afterward into 14 bit digitizers. The net quantum efficiency of this camera was $\approx$30%, its dynamic range was 1000, and its readout noise was $\approx$20 electrons/pixel.

A typical sequence of images from the PSI-3 camera is shown in Fig. 8. This sequence was taken at 4 μs/frame using the same GPI field of view as for Fig. 2, and shows the movement of two localized maxima or ''blobs'' of D_α light emission. Such blobs were seen to move poloidally or radially at a speed of up to $\approx$1 cm/20 μs ($\approx$500 m/s), but such blobs could also come and go without much movement, and sometimes the movement seemed to be more ''wave-like'' with a phase speed mainly in the ion diamagnetic direction. The autocorrelation time at a single point in these images was $\approx$10–20 μs, consistent with the time series measurements made using the fast diodes (see Fig. 5). Videos of these images can be viewed at http://www.pppl.gov/~szweben/.

It is possible that these moving ''blobs'' are examples of coherent structures analogous to those seen in turbulent neutral fluid flow.[8] Minor radius sized coherent structures have previously been measured in a low-temperature toroidal plasma,[25] and smaller-scale ''blobs'' or ''intermittent structures'' have previously been identified using Langmuir probe data in tokamaks,[17,26–29] and are being analyzed theoretically.[30,31] Further analysis of the motion in these images will be presented elsewhere.

IV. COMPARISON WITH THEORETICAL SIMULATION

Numerical simulations of edge turbulence in C-Mod were made with a 3D nonlinear electromagnetic two-fluid model which was developed specifically to treat the collisional edge plasma of tokamaks.[4,7] This model is based on the Braginskii equations and has both diamagnetic and toroidal curvature effects, but does not have kinetic effects like Landau-damping or nonthermal distribution functions. The simulation described below was carried out in a shifted-circle closed field line magnetic geometry, and thus, in contrast to the geometry of the experiment, has no magnetic separatrix or limiters. At least qualitatively, we expect this approach to be a reasonable first step, since in the present case the com-

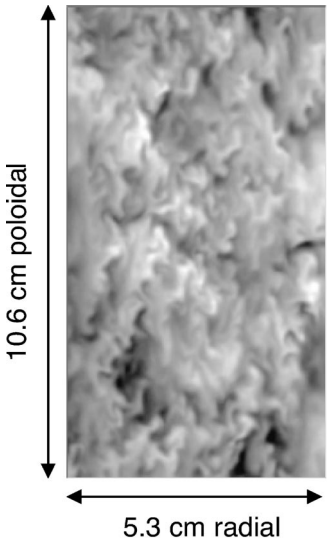

FIG. 9. Typical image from the numerical simulation of edge turbulence in C-Mod. The local brightness of this image is proportional to the local density fluctuation normalized to the average density at each point. This simulation is ''local'' in the sense that it models only the plasma parameters and local gradients at a point $\rho=0.5$ cm outside the separatrix (see Table I for parameters). The radial domain of the code is made larger than the domain over which these parameters are constant in the actual profile shown in Fig. 4(b).

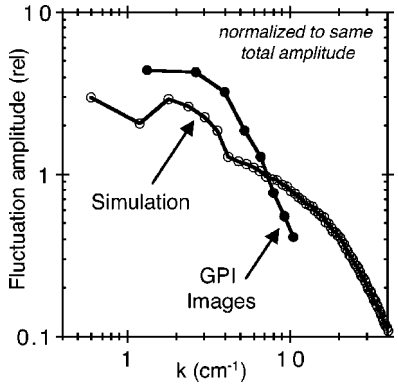

FIG. 10. Initial comparison of the *k*-poloidal spectra calculated from the simulation code and the GPI images for the same discharge (#1010622006), normalized to have the same total fluctuation amplitude for clarity. Although the mean correlation lengths of the simulation and the data are similar, the *k* spectrum from the simulation has relatively more amplitude at high-*k* than does the data.

bined effect of magnetic shear ($\hat{s}=1.3$) and unfavorable curvature localizes the turbulence on the outboard midplane. It is also a ''local'' simulation in the sense that the background gradients of the density and temperature are assumed to be constant throughout the simulation domain and the density and temperature fluctuations are assumed to be small compared to the background values.

A typical pattern of density fluctuations as calculated by this code for a C-Mod edge plasma is shown in Fig. 9. This case was run for the $B=5.4$ T, $I=1.0$ MA plasma of Fig. 4(b) at a point 0.5 cm outside the separatrix where $n_e=2.5\times10^{13}$ cm^{-3} and $T_e=24$ eV (see Table I). The simulation domain in Fig. 9 is 5.3 cm radially by 10.6 cm poloidally, i.e., has many wavelengths in both the poloidal and radial directions, with periodic boundary conditions in the poloidal direction and outwardly decaying conditions for the turbulence and fixed values for the background at the radial boundary. The code was started from initial noise, progressed through a linear instability phase dominated by the resistive ballooning mode, and reached a saturated steady state at around 40 μs (the time of Fig. 9 is around 100 μs).

The poloidal correlation length of the density fluctuations in this simulation is $L_{\rm pol}=0.6\pm0.1$ cm, which is roughly consistent with the GPI imaging result of $L_{\rm pol}=0.85\pm0.2$ cm. Similarly, the local fluctuation level in the simulation was $\delta n/n=0.18$ and $\delta T_e/T_e=0.13$, with δT_e in phase with δn. This fluctuation level is within a factor of 2 of that seen by the GPI diodes but somewhat smaller than that seen in the Langmuir probes (Fig. 6). The predicted particle diffusion coefficient of $D=0.2$ m^2/s from the simulation is within about a factor of 2 of the experimental estimate for that part of the scrape-off layer.[17]

There are, however, notable differences, which appear to stem from the fact that the simulation contains more small-scale structure than does the GPI images. A comparison of the *k*-poloidal spectra calculated from the simulation and from the GPI images for the same discharge is shown in Fig. 10. In this figure the $k_{\rm pol}$ spectral amplitude of δn from the simulation is plotted against the $k_{\rm pol}$ spectral amplitude from the GPI images within $\rho=0.5\pm0.3$ cm outside the separatrix (these images were taken at 2 μs exposure as described in Sec. III B). At this radius the GPI should respond as $S_{D_\alpha}\propto n_e^{0.5}\,T_e^{0.5}$ (Sec. II B), so if the density and temperature fluctuations are in phase and similar in magnitude (as suggested by the simulation), the GPI *k* spectrum should also be approximately that of δn. For clarity, the two curves are normalized so as to have the same total fluctuation amplitude. It is seen that, despite the similarity in the average correlation length of the simulation and GPI data, the shapes of the two *k* spectra are different, with the simulation having more small-scale structure up to the fastest growing resistive ballooning mode near $k_{\rm pol}=30$ cm^{-1}.

The relative excess of high wave numbers in the simulation also leads to a discrepancy between the predicted and observed correlation times. The autocorrelation time in the simulation was 5.6 μs FWHM (full-width-half-maximum), while that measured by the GPI diodes was 10–20 μs FWHM. Averaging the simulation data over a period of 4 μs reduces the fluctuations at $k=6$ cm^{-1} by a factor of 1.8 while hardly affecting the fluctuations at $k=2$ cm^{-1}. From the theoretical point of view, a reduction of the small space and time scales in the simulation could arise from some additional small scale diffusion or viscosity that is not present in the Braginskii simulation model. Such damping, when artificially added to the simulations, has little impact on the predicted transport, which arises mainly from the larger scales. The physical origin of such damping, however, is not clear (the charge exchange or ionization of neutrals and finite Larmor radius effects can probably be ruled out as a source of such damping, because of their smallness). On the experimental side, the strong decay at small scales could potentially be due to an unknown factor reducing either the space

or time resolution of the diagnostic to about ≈ 1 cm or ≈ 4 μs, respectively.

Thus the initial comparison of the theoretical simulation with the measured edge turbulence in C-Mod is encouraging in several respects; namely, that the average length scales, fluctuation amplitudes, and diffusion coefficients in the local simulation agree to within about a factor of 2 with the local measurements just outside the separatrix. However, the turbulence autocorrelation times and k_{pol} spectrum shapes appear to be significantly different. Clearly more work needs to be done to track down the source of these discrepancies. The reliability of the Braginskii model at the shorter scales can be tested by comparing the fluid results to kinetic descriptions. The simulations could also be improved by including more realistic boundary conditions[5,32] and nonlocal effects.[7] Finally, improvements can be made in the experiment by increasing the *k*-spectral range and by using DEGAS 2 to help interpret the fluctuations.

V. SUMMARY

This paper describes the initial results from a gas puff imaging technique for 2D visualization of edge plasma turbulence in the Alcator C-Mod tokamak. These images show a highly turbulent structure in the radial vs poloidal plane perpendicular to the main magnetic field near the outer midplane separatrix. A statistical analysis of the images shows a mean poloidal correlation length of $L_{\mathrm{pol}} \approx 0.85 \pm 0.2$ cm in the edge region extending from roughly 2 cm outside to 1 cm inside the separatrix. This size scale agrees fairly well with the edge turbulence simulation result of $L_{\mathrm{pol}} \approx 0.6 \pm 0.1$ cm. The motion of this 2D structure was also captured using an ultrahigh speed camera and often showed isolated maxima or ''blobs'' moving through the plasma edge.

There are many avenues for improvement on the present results. In the area of diagnostics, the relative n_e and T_e fluctuations might be measured by imaging two different spectral lines simultaneously, while the motion of the turbulence could be seen better using a new 312-frame ultrafast camera being developed by PSI. Experimentally, it would be useful to extend the GPI viewing region a bit farther inward to better characterize the *H*-mode barrier region and the density limit. Finally, the comparisons with theory could be improved by doing systematic scaling experiments along with a more detailed analysis of the structure and motion of the turbulence. With these and other relatively straightforward techniques it should be possible to understand the physics of edge turbulence in tokamaks.

ACKNOWLEDGMENTS

The authors acknowledge valuable discussions and support for this work from G. Antar, J. Boedo, R. Boivin, D. D'Ippolito, J. F. Drake, G. Hammett, T. S. Halm, D. Johnson, S. Krasheninnikov, B. Lipschultz, E. Marmar, J. Myra, W. Nevins, G. Schilling, D. Simon, G. Tynan, S. Wolfe, and X. Xu.

This work was performed under U.S. DOE Contract No. DE-AC02-CHO3073.

[1] M. Endler, J. Nucl. Mater. **266–269**, 84 (1999).
[2] B. A. Carreras, IEEE Trans. Plasma Sci. **25**, 1281 (1997).
[3] A. J. Wootton, B. A. Carreras, H. Matsumoto, K. McGuire, W. A. Peebles, C. P. Ritz, P. W. Terry, and S. J. Zweben, Phys. Fluids B **2**, 2879 (1990).
[4] B. N. Rogers, J. F. Drake, and A. Zeiler, Phys. Rev. Lett. **81**, 4396 (1998).
[5] X. Q. Xu, R. H. Cohen, T. D. Rognlien, and J. R. Myra, Phys. Plasmas **7**, 1951 (2000).
[6] F. Jenko and B. D. Scott, Phys. Plasmas **6**, 2705 (1999).
[7] K. Hallatschek and A. Zeiler, Phys. Plasmas **7**, 2554 (2000).
[8] U. Frisch, *Turbulence* (Cambridge University Press, Cambridge, MA, 1995).
[9] S. J. Zweben and R. W. Gould, Nucl. Fusion **23**, 825 (1983).
[10] G. R. McKee, R. Ashley, R. Durst, R. Fonck, M. Jakubowski, K. Tritz, K. Burrell, C. Greenfield, and J. Robinson, Rev. Sci. Instrum. **70**, 913 (1999).
[11] R. J. Maqueda, G. A. Wurden, S. J. Zweben, L. Roquemore, H. Kugel, D. Johnson, S. Kaye, S. Sabbagh, and R. Maingi, Rev. Sci. Instrum. **72**, 931 (2001).
[12] J. L. Terry, R. Maqueda, C. S. Pitcher, S. J. Zweben, B. LaBombard, E. S. Marmar, A. Y. Pigarov, and G. Wurden, J. Nucl. Mater. **290**, 757 (2001).
[13] R. L. Boivin, J. W. Hughes, B. LaBombard, D. Mossessian, and J. L. Terry, Rev. Sci. Instrum. **72**, 961 (2001).
[14] S. J. Zweben, J. McChesney, and R. W. Gould, Nucl. Fusion **23**, 825 (1983).
[15] M. Endler, H. Neidermeyer, L. Giannone, E. Holzhauer, A. Rudyj, G. Theimer, and N. Tsois, Nucl. Fusion **35**, 1307 (1995).
[16] S. J. Zweben and S. S. Medley, Phys. Fluids B **1**, 2058 (1989).
[17] B. LaBombard, R. L. Boivin, M. Greenwald, J. Hughes, B. Lipschultz, D. Mossessian, C. S. Pitcher, J. L. Terry, and S. J. Zweben, Phys. Plasmas **8**, 2107 (2001).
[18] D. P. Stotler, C. S. Pitcher, C. J. Boswell, T. K. Chung, B. LaBombard, B. Lipschultz, J. L. Terry, and R. J. Kanzleiter, J. Nucl. Mater. **290–293**, 967 (2001).
[19] M. A. Meier, R. D. Bengtson, G. A. Hallock, and A. J. Wootton, Phys. Rev. Lett. **87**, 085003 (2001).
[20] T. Auguste, M. Bougeard, E. Caprin, P. D'Oliviera, and P. Monot, Rev. Sci. Instrum. **70**, 2349 (1999).
[21] M. A. Pedrosa, I. Garcia-Cortez, B. Branas, R. Balbin, C. Hidalgo, L. Schmitz, G. Tynan, A. Post-Zwicker, and the PBX-M Team, Phys. Plasmas **2**, 2618 (1995).
[22] B. Kurzan, S. D. Hempel, E. Holzhauer, B. Scott, F. Serra, W. Suttrop, and A. Zeiler, Plasma Phys. Controlled Fusion **42**, 237 (2000).
[23] C. E. Bush *et al.*, ''Evolution and termination of H-modes in NSTX,'' to be published in Plasma Phys. Controlled Fusion.
[24] J. L. Lowrance and W. F. Kosonocky, Proc. SPIE **2869**, 405 (1997).
[25] O. Grulke, F. Greiner, T. Klinger, and A. Piel, Plasma Phys. Controlled Fusion **43**, 525 (2001).
[26] G. Y. Antar, S. I. Krasheninnikov, P. Devynck, R. P. Doerner, E. M. Hollmann, J. A. Boedo, S. C. Luckhardt, and R. W. Conn, Phys. Rev. Lett. **87**, 065001 (2001).
[27] J. A. Boedo, D. Rudakov, R. Moyer *et al.*, Phys. Plasmas **8**, 4826 (2001).
[28] B. A. Carreras, V. E. Lynch, and B. LaBombard, Phys. Plasmas **8**, 3702 (2001).
[29] S. J. Zweben, Phys. Fluids **28**, 974 (1985).
[30] S. I. Krasheninnikov, Phys. Lett. A **283**, 368 (2001).
[31] D. D'Ippolito, J. R. Myra, and S. I. Krasheninnikov, Phys. Plasmas **9**, 222 (2002).
[32] Y. Sarazin and Ph. Ghendrih, Phys. Plasmas **5**, 4214 (1998).